IEEE Open Journal of the
Industrial Electronics Society

Received 8 March 2021; revised 15 April 2021; accepted 22 April 2021. Date of publication 27 April 2021;
date of current version 19 May 2021. The review of this article was arranged by Associate Editor Oscar Lucia.

Digital Object Identifier 10.1109/OJIES.2021.3076137

A New Method for Offline Compensation of Phase Discrepancy in Measuring the Core Loss With Rectangular Voltage

NAVID RASEKH (Student Member, IEEE), JUN WANG (Member, IEEE), AND XIBO YUAN (Senior Member, IEEE)

Department of Electrical and Electronic Engineering, University of Bristol, Bristol BS8 1UB, U.K

CORRESPONDING AUTHOR: XIBO YUAN (e-mail: xibo.yuan@bristol.ac.uk).

This work was supported in part by the U.K. Royal Academy of Engineering.

ABSTRACT Nowadays accurate characterization of the magnetic component losses becomes increasingly important in the design stage of power converters. As the main challenge in characterizing a magnetic component, the core loss is commonly measured through the two winding *B-H* loop measurement method that is susceptible to the phase discrepancy error, especially for low-permeability, low-loss cores. This paper, therefore, proposes a new offline method to compensate the phase discrepancy error in high-frequency core loss measurement under rectangular voltage excitation. In the post-processing of measured waveforms, the phase discrepancy is compensated by shifting the measured current horizontally to align with a reference phase angle, which is found from an offline impedance sweep on the component-under-test and FFT analysis. As a result, the testing voltage and current waveforms can be measured without considering deskew at the time of measuring. Additionally, this method is more accurate than calibration methods considering a fixed frequency response (e.g., a deskew fixture), because it considers the frequency response across the whole spectrum. The proposed approach can be well applied for typical PWM converters with switching frequencies up to hundreds of kilohertz, for which the effective voltage harmonics extend to a few megahertz range that can be well evaluated with an impedance analyzer. The presented method is experimentally verified against the existing partial cancellation method which is immune to phase discrepancy error.

INDEX TERMS B–H loop measurement, core loss, phase discrepancy error, magnetic losses, two-winding method.

I. INTRODUCTION

Substantial advancement in high-speed, low-loss power semiconductors enabled by the wide-bandgap material has been pushing power converters to higher frequencies and higher power densities in the past decade. Alongside the development of power semiconductors, magnetic components and their high-frequency losses, especially the core loss, have a considerable impact on the converter efficiency, power density and temperature rises, which calls for accurate characterization and modelling. To characterize the core loss, there are mainly two ways, in general, to measure it empirically: the electrical method [1]–[4] and the calorimetric (thermal) method [1], [4], [5]. The principle of the calorimetric method is to enclose the component-under-test with a near-adiabatic calorimetric container and measure the temperature rise between the inlet and outlet coolant to deduct the generated loss of the magnetic component. The calorimetric method is in general reliable and insensitive to the electrical noises and parasitics in the measurement instruments, but its main drawback is the time-consuming process to reach the thermal steady-state, which makes it difficult to measure the high-frequency loss in a relatively short transition. Also, if the interest is the core loss alone, a complicated procedure needs to be applied to exclude the winding loss from the measured total loss of a magnetic component [1], [4], [5]. Therefore, the electrical techniques are still commonly implemented over the thermal methods due to the above limitations.

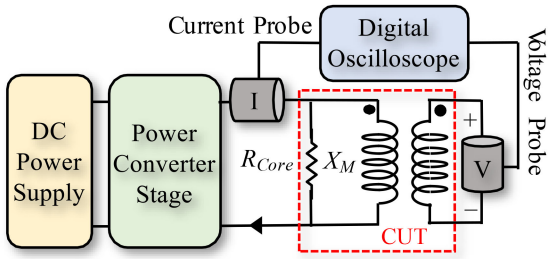

FIGURE 1. Two-winding measurement method.

To characterize the high-frequency dynamic core losses, the two winding method as an electrical method is used extensively and considered as a universal process [2]. The core loss measurement with two winding method is realized by integrating the product of the open-circuit voltage drop v_{Sec} across the secondary winding (sensing winding) of the magnetic component under test (CUT) and the current i_{Pri} flowing through the primary winding as defined in (1)

$$P_{Core} = \frac{N_1}{N_2}\frac{1}{T}\int_0^T i_{Pri}(t)\cdot v_{sec}(t)\,dt \tag{1}$$

where T is the period of one cycle; N_1 and N_2 are the numbers of the primary and secondary winding turns, respectively. These signals are captured by the probes and digital oscilloscope over time as shown in Fig. 1. The superiority of the two winding method is that it is simple to implement and applicable for arbitrary wave excitation in both steady-state and transient measurements, while it only measures the core loss and excludes the copper loss [3]. However, the two winding method is sensitive to the phase discrepancy as extensively reported in [3], [4], which is the difference between the true and measured phase shift between i_{Pri} and v_{Sec}. This phase error is typically caused by the oscilloscope sampling resolution, trigger jitter, sensing resistor parasitic inductance, or probes delay time, depending on the current sensing method, which can further deteriorate at higher frequencies. The presence of the phase discrepancy error is significant in the case of low permeability or gapped cores and low loss cores [4]. Hence, the phase discrepancy issue should be carefully addressed in high-frequency two-winding measurements.

Previous studies proposed several ways to compensate the phase discrepancy error for the two winding method. One direction is to apply the reactive voltage cancellation concept. Authors in [6] firstly proposed to use a capacitor to resonate completely with the magnetizing inductance of the CUT and tune out the reactive voltage to have an equivalent loss resistance to diminish the sensitivity of the phase discrepancy. However, this method suffers from the distortions in the case of the high amplitude of excitation and the requirement of different capacitors for each testing conditions [6]. [7] improved this approach by applying a series capacitor to precisely resonate with the CUT at the fixed system frequency. However, it is complex for this method to exclude the winding loss to find the exact core loss and challenging to find the core loss under a specific dc-biased current. Besides, this method is limited to sinusoidal excitation, and it is an arduous task to change the capacitor for every testing point with various resonant frequencies.

Mu's capacitive and inductive cancellation methods in [4], [8], [9] further improved the previous methods and combined them with the two winding method to exclude the winding loss. The concept is to remove the reactive voltage of the CUT by reducing θ from closely 90° to nearly 0°. Although the capacitive method [4] is still only used for sinusoidal excitation, by replacing the capacitor with an air-core or low core loss transformer, the inductive method can be utilized for any arbitrary excitation waveforms [8], [9]. However, as the drawback of Mu's approaches, the reference capacitor's capacitance and the reference transformer's magnetizing inductance are pivotal values, for which a small mismatch from the perfect cancellation will lead to a substantial error [10]. Furthermore, it is a time-consuming process to delicately tune the capacitor or transformer for various testing conditions.

Hou's partial cancellation concept was brought up in [10] as an extension of Mu's method. The fundamental concept of this method is to utilize the phase shift seen on the air-core transformer to offset the phase shift seen in the measurement of the CUT loss. As demonstrated in [10], the requirement of the fine-tuned value of the cancellation component is minimized in this method. However, this method is only effective for systems with lower frequencies (e.g., < 5 MHz) compared to Mu's method, due to the considerable reference core loss errors [11], [12]. Furthermore, both Hou's and Mu's inductive cancellation methods are only applicable when the magnetizing inductance of CUT is relatively low (e.g., $<$ a few hundreds of nano-henries). If the magnetizing inductance of the matching air-core transformer needs to be high, its parasitic inductance and capacitance becomes significant, which can have adverse effects on the waveforms and system accuracy [13].

A de-skew fixture is also available from the manufacturers of oscilloscopes and probes, e.g., Keysight U1880A, which can be used to calibrate the time delay between current and voltage probes. The compensation is reflected in the deskew function of the oscilloscopes to shift the waveforms horizontally. Although the calibration is performed with rectangular waveforms, this calibration is conducted with a fixed square wave with fixed frequency and rising/falling slopes. As a consequence, there are still potential small errors and delay times at other frequencies [14], [15]. In addition, the calibration is typically conducted manually, which is subject to human objective error. Also, the de-skew tool board still has parasitic elements itself and may affect the calibration procedure [16].

Shimizu et al. proposed a technique in [17], [18] to compensate the phase discrepancy error in two-winding core loss measurement. In this method, a phase error of the measuring system is found with a reference low-inductance resistor. This phase error at each frequency of sinusoidal excitation is the phase difference between the phase angle measured by the

B-H analyzer and the reference response of the resistor that is separately evaluated by an impedance analyzer. This extracted phase error is then fitted to a function and saved in the *B-H* analyzer to correct the phase angle of measured current on each frequency harmonic through a Fourier function. The accuracy of this method is verified against a power meter. However, the reference noninductive resistor in this approach is considered to have a linear impedance characteristic (constant parasitic inductance) while its capacitive component is ignored, which may introduce nonlinearity in the high-frequency range. Also, the impedance characterization is only conducted to 500 kHz in [17], [18].

To offer an alternative to compensate the phase discrepancy in core loss testing, a new offline method is proposed in this paper as the contribution. The proposed approach is to find the reference phase shift through an offline impedance frequency sweep on the magnetic-component-under-test using an impedance analyzer, and harmonic analysis of the measured testing voltage by fast Fourier transform (FFT). In short, the proposed method shifts the current waveform horizontally in the offline post-processing utilizing a separately obtained reference phase shift to align to the physical phase shift and reduce the phase discrepancy error. Compared with existing approaches, the proposed method requires no additional cancelling components and can be conducted without considering deskew at the time of measuring the waveforms. This approach can accurately measure the magnetic component losses in a wide frequency range. The proposed approach can be well applied for typical PWM converters with switching frequency up to hundreds of kilohertz, for which the effective harmonics extend to a few megahertz range that can be well evaluated with an impedance analyzer.

Section II explains the phase discrepancy issues in the two winding method. The proposed procedure is then discussed in Section III and experimentally verified in Section IV.

II. PHASE DISCREPANCY ISSUE IN TWO-WINDING MEASUREMENT

As derived in [3], the relationship between the core loss measurement error in percentage with regards to the phase discrepancy can be found by (2) for sinusoidal excitation:

$$E = \frac{P_{\text{Measured}} - P_{\text{Physical}}}{P_{\text{Physical}}} \times 100\% = \frac{\cos(\theta+\alpha) - \cos(\theta)}{\cos(\theta)} \times 100\% \quad (2)$$

where E is the relative error in percentage of the measured core loss, θ is the actual phase shift in degrees between i_{Pri} and v_{Sec}, α is the phase error in the measurement of θ in degrees, and $P_{Measured}$ and $P_{Physical}$ are the measured core loss value and the real core loss value, respectively. The relative error E is sensitive to both θ and α. It can be seen in (2) that when θ is near 90°, the relative core loss measurement error E can become significant even with a small α, mainly because the denominator (the real core loss) is approaching zero. Equations (3) to (5) demonstrate how the low permeability, low loss cores influence the phase shift error [14], [15].

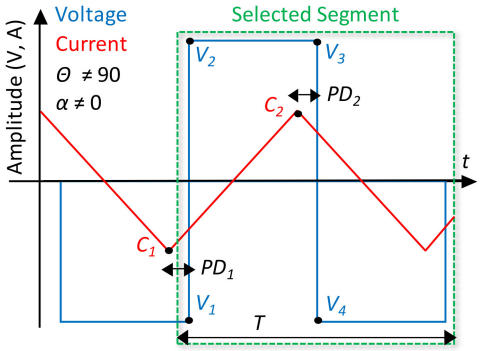

FIGURE 2. CUT waveforms when the α is not zero.

$$R_{Core} \propto \frac{1}{P_{Core}} \quad (3)$$

$$X_M = 2\pi f L = 2\pi f \frac{N^2 \mu A_e}{l_e} \quad (4)$$

$$\theta = \arctan\frac{R_{Core}}{X_M} \propto \arctan\left(\frac{1}{\mu P_{Core}}\right) \quad (5)$$

where R_{Core} represents the core loss resistance, reactance X_M is the magnetizing impedance of the CUT, f is the operating frequency, L is the magnetizing inductance, A_e is the core cross-section area, l_e is the average magnetic length, μ is the core permeability, and N is the number of winding turns assuming N=N1=N2 for simplicity. Equation (5) shows the dependence of the θ on material properties, i.e., the core permeability and core loss value, which shows θ and subsequently the phase discrepancy sensitivity will be enlarged when the CUT has lower values for μ and P_{Core}.

These equations used in previous works are based on sinusoidal waveforms, while power converters mostly operate under rectangular excitation voltages. Therefore, the phase error distinctions between these two types of waveforms are also evaluated in this work. Fig. 2 shows the typical CUT voltage and current with a rectangular excitation voltage waveform and a slightly leading current ($\theta < 90°$).

In power electronics applications, the CUT current can contain a dc component. which can impact the dynamic core loss and core permeability [19]. In (5), the core loss and core permeability are correlated to the actual phase shift θ, which will subsequently correlate to the calculated relative error in (2). Note the dc-bias inherently does not affect the physical phase shift of the measured waveforms. The dc-bias current only shifts the current in the vertical axis, and its impact on the core loss is reflected as the dynamically changing permeability resulting in the more curvy shape of the current [20] rather than the change of phase angle.

The voltage is chosen as the reference of phase angles α and θ. When $\alpha = 0°$ and $\theta = 90°$, the rising/falling edge of

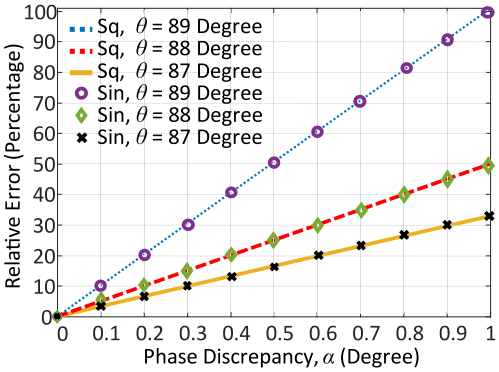

FIGURE 3. Loss measurement relative error in the variation of α for square (Sq) and sinusoidal (Sin) voltage excitations in the different values of θ.

the voltage is aligned to the trough/peak point of the current and it can be expected that the measurement gives the real loss value, which is zero in this case. When α is negative, the measurement error becomes positive and the obtained loss is higher than the real loss. Vice versa, if α is positive, the measurement error becomes negative, and the measured loss is lower than the actual core loss.

Fig. 3 illustrates the calculated relative error E when the α changes between zero to one degree for both sinusoidal and rectangular excitation and various θ. The first observation is that the phase shift error for square excitation shows little difference to the sinusoidal case. As the second observation, it should be highlighted that when θ is fixed, the relative error E is linearly proportional to the phase discrepancy α. Although the slopes in Fig. 3 seems steeper at a higher θ, this is due to the denominator in (2) approaching zero as θ approaching 90°. In other words, the sensitivity between the measured core loss and the phase discrepancy α is a linear relationship for one measurement point, which is also reported in [21], [22]. The analysis above for the square wave is conducted with the duty cycle of the excitation voltage of 50%. The sensitivity of two winding method as well as phase-shift error for other duty cycles can further increase as investigated in [13].

As introduced, the main cause of the phase discrepancy error in measuring core loss with the two-winding method is the current measuring instrument. In the next section, a novel approach will be presented to compensate this phase discrepancy error.

III. PROPOSED OFFLINE COMPENSATION METHOD OF PHASE DISCREPANCY

For characterizing the core loss, existing methods experimentally measure it through either sinusoidal or rectangular excitation voltages [23]–[27]. Recently, the loss map approach introduced in [18], [20] advocates measuring the core loss with rectangular excitation voltage and dc-biased current, which is state-of-the-art progress. For measuring the core loss as well as creating a loss map with the two winding method, the phase discrepancy as the major concern will be compensated with a novel method as follows.

A. CORE LOSS MEASUREMENT

In the two-winding method, the core loss is obtained by integrating the product of the secondary voltage and the primary current of the CUT, which reflects the area of a closed B–H loop. To excite the CUT, a half-bridge structure proposed in [28]–[30] is utilized in this work, which is shown with the experiment setup in Appendix A. A discontinuous test procedure called triple pulse test (TPT) is applied, which is proposed in [28], [29]. The concept of TPT is to test limited cycles only and prevent unnecessary continuous operations. The temperature in TPT is easy to control because it does not introduce any temperature rise in the testing due to the short testing transition.

In this work, three types of popular core material are characterized through three sample inductors. Their rated inductances are selected at around 100 μH to have similar magnetizing inductances in the frequency range between 10 to 100 kHz. The waveforms are measured by high-bandwidth voltage and current probes. The specifications of the instruments, inductors and other test rig components are shown in Appendix A. As discussed in [28], [29], the number of required cycles for TPT may differ depending on the CUT. This work used four pulses to stabilize the CUT to reach the steady-state. The core loss is measured with zero dc-biased currents in this section for simplicity, because the dc-bias current itself does not affect the phase shift of the probes and inductor waveforms, and the peak value of the measured signal has no impact on the phase discrepancy error [15]. The B-H loop is found from the measured signals, for which the detailed formulas can be found in Appendix A. Fig. 4(a) depicted the experimental TPT result for the iron powder inductor with 50 kHz frequency and ±50 V inductor voltage, for which the selected segment is magnified in Fig. 4(b). Fig. 4(c) illustrates the corresponding flux density swing (ΔB) for the iron powder core at 50 kHz, in which the alignment of the black dots proves that the system reached the steady-state for the selected cycle. The measured core losses of the CUTs in the frequency range of 10 to 100 kHz are shown in Fig. 5. While surveying various frequencies, the applied inductor voltage is kept constant (e.g., 50 V) regardless of the frequency increment, which leads to the reduction in flux density swing at higher frequencies. Hence, the core loss decreases with the increase of the frequency in Fig. 5 due to smaller ΔB at higher frequencies. Additionally, the N87 at 10 kHz and N30 at 10 and 20 kHz are saturated due to the large value of their ΔB. Therefore, these results are omitted from Fig. 5.

However, the measured loss is not the real loss that the physical circuit has, owing to the phase discrepancy error, and as a consequence, the value of the probe phase discrepancy α is not easy to recognize during the measurement. By phase-shifting the current deliberately, Fig. 6 illustrates how the core loss changes as α (skew) varies. This figure shows the relation between the core loss and α is linear, rather than

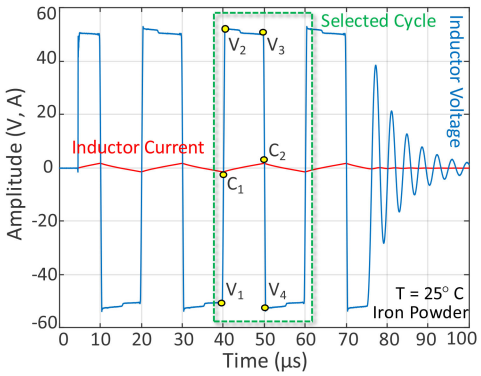

(a)

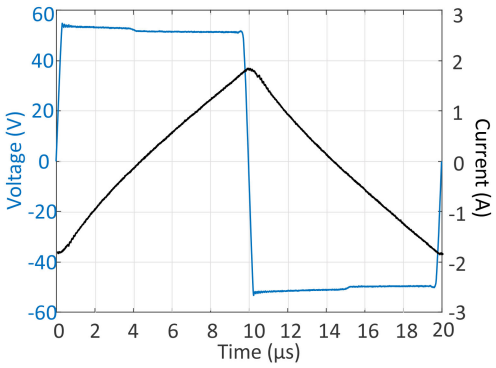

(b)

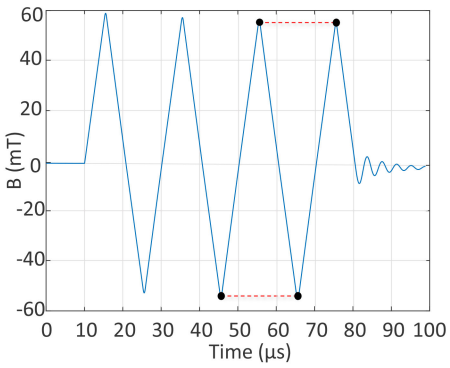

(c)

FIGURE 4. **Experimental TPT result for iron powder at 50 kHz frequency, (a) whole process, (b) selected segment magnification, (c) flux density waveform.**

an exponential relationship, as analyzed in Section II. For example, for the case of 50 kHz in Fig. 6, the core loss with regard to the skew value can be expressed as

$$\text{Core Loss (W)} = 7.7 + 0.045 \cdot \text{Skew (ns)} \tag{6}$$

Therefore, the reference zero skew that the oscilloscope is assumed and depicted in Fig. 6 is not the zero skew in the actual system. The accurate position of real physical timing

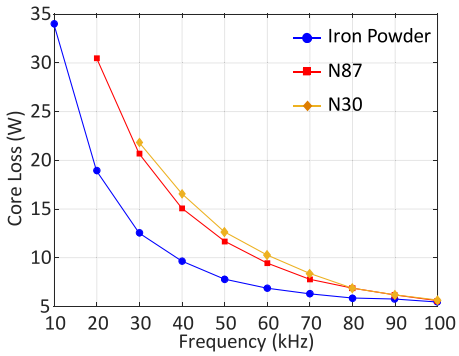

FIGURE 5. **The core losses of the varied CUTs at the different frequencies range, T = 25° C.**

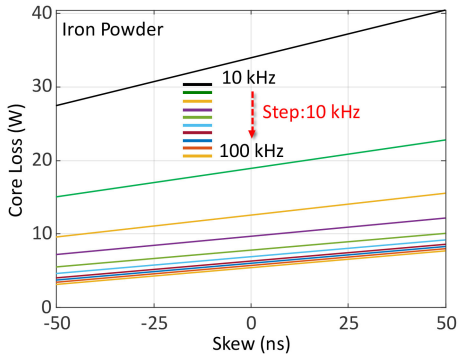

FIGURE 6. **Core loss measurement for iron powder vs. timing skew, T = 25° C.**

skew is considered unknown [21], [22]. The following sections explain how to find a reference deskew value to compensate it.

B. FINDING THE MEASURED UNCALIBRATED PHASE SHIFT (PD)

With the voltage and current waveforms measured in the TPT, the phase difference, *PD,* between the voltage and current can be found as shown in Fig. 2. In Fig. 2, t_{V1} and t_{V3} are the moments (time) when the CUT voltage starts rising and falling, respectively. t_{V2} and t_{V4} are the moments when the CUT voltage completes the rising and falling process, respectively. t_{C1} and t_{C2} are the moments that the current reaches the lowest (minimum) and highest (peak) value, respectively. Therefore, PD_1 and PD_2 are the voltage and current phase differences, which should be similar to each other. PD_1 and PD_2 contain the physical (real) phase shift, plus the instruments' phase discrepancy, which can be found as

$$PD_1\,(time) = \left(\frac{t_{V1} + t_{V2}}{2}\right) - t_{C1} \tag{7}$$

$$PD_2\,(time) = \left(\frac{t_{V3} + t_{V4}}{2}\right) - t_{C2} \tag{8}$$

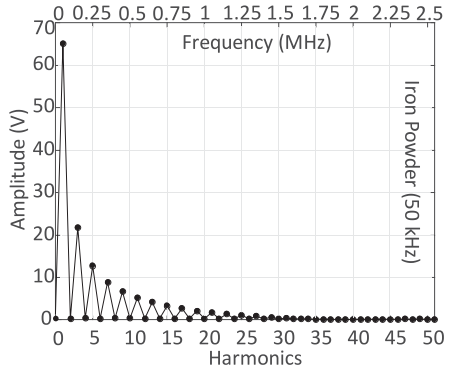

FIGURE 7. Fourier analysis *Vsec(n)* of one selected rectangular voltage cycle shown in Fig. 4(b) of the 50 kHz rectangular voltage.

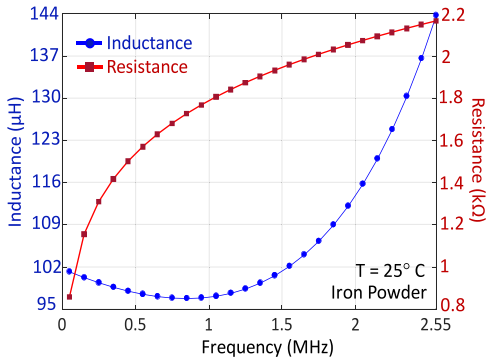

FIGURE 8. Inductor impedance spectrum $Z_{L(n)}$ ploted in resistance and inductance.

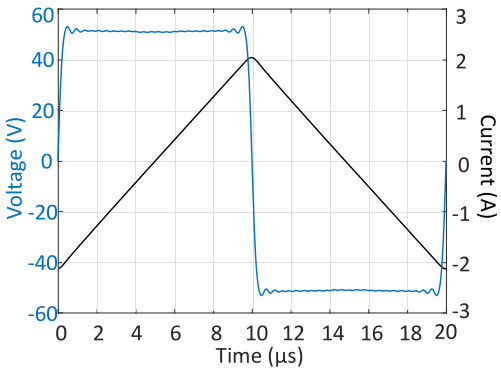

FIGURE 9. Regenerated iron powder voltage and current waveforms at 50 kHz frequency for the selected segment of TPT.

The reason for using the t_{V1} to t_{V4} instead of the voltage zero crossing moments is that the inductor voltage may have a dc offset. Besides, since the experimental voltage rising or falling edges are not completely straight lines, by averaging between the t_{V1}, t_{V2} or t_{V3}, t_{V4}; the voltage and current phase differences (PD_1 and PD_2) are captured more reliably. Finally, to minimize the probable errors, by averaging PD_1 and PD_2, the experimental uncalibrated phase shift (PD) is calculated as

$$PD = \frac{1}{2}(PD_1 + PD_2) \tag{9}$$

To minimize the impact of random measurement errors, e.g., noises, the TPT result at each excitation frequency is the mean of 16 repeated runs in this work. Based on experimental observation, 16 samples is sufficient to result in smooth waveforms to accurately work out the core loss and uncalibrated phase shift PD. Increasing the number of samples any further does not significantly change the results anymore.

C. FINDING THE REFERENCE PHASE SHIFT (PS_REF)

After finding the uncalibrated phase shift (PD), the next step is to find the reference phase shift (PS_Ref) so that the waveforms can be manipulated to move towards the physical phase shift (PS). Firstly, by performing fast Fourier transform (FFT), the amplitudes of each harmonic of the inductor voltage shown in Fig. 4(b) can be found for one cycle. Fig. 7 displays the FFT results in the frequency domain from the selected segment of voltage at 50 kHz. In this case, the FFT is calculated up to the 51st harmonic, since the amplitude of the further harmonics converges to zero as shown in Fig. 7.

The next step is to perform an impedance frequency sweep through a precision impedance analyzer, e.g., Wayne Kerr 6500B in this work. Fig. 8 shows the impedance of the iron powder inductor at each frequency ($Z_{L(n)}$), when the impedance analyzer assumes the components (resistance and inductance) are connected in parallel.

To protect the accuracy of impedance measurement at the frequency level of a hundred MHz, it is ensured that no large metal objects are near the magnetic component during the measurement [31]. According to the impedance analyzer datasheet, the measurement accuracy of impedance is ±0.05% with frequencies up to 120 MHz. As can be seen from Fig. 7, the effective harmonic component of the typical rectangular voltage seen in PWM converters would typically reach several MHz, which is mainly contributed by the rising/falling edge of the PWM waveform. Therefore, a small discrepancy in the very high-frequency region (e.g., 100 MHz) will not impact the accuracy. Moreover, by virtue of TPT, both the experiment and impedance analyzer procedures are performed at room temperature (T = 25° C), which avoids the discrepancy caused by the temperature factor.

After finding the impedance spectrum and the experimentally applied voltage on CUT, a virtual current i' on the inductor can be regenerated through (10) by adding up the current responses from each frequency/harmonic. An elaboration of the equation can be found in Appendix B.

$$i' = \sum_{n=1}^{n=\infty} \frac{V_{(n)}}{Z_{L(n)}} \tag{10}$$

Fig. 9 depicted the regenerated iron powder voltage and current waveforms at 50 kHz. By identifying the peak point of the regenerated inductor current in Fig. 9, a reference phase shift (PS_Ref) in nanoseconds can be found. Locating the peak

point moment in this stage is easier compared to analyzing the experimental waveform, which is implemented by detecting the highest value of the regenerated current in the coding and recording the corresponding time stamp.

The final step is to horizontally shift the experimentally measured current to the point where its phase shift with regard to the inductor voltage equals to the reference *PS_Ref*. This step is performed in MATLAB by applying a horizontal offset *PS_Com* (=*PD* – *PS_Ref*) on the current waveform. This step is similar to the de-skew function on the oscilloscope, which applies a time offset (horizontal axis) on one channel of signal in relative to the reference. The current can be shifted like Fig. 6 for each frequency to find the core loss. Hence, by calculating the equation of each line function and knowing the *PS_Com* value, the new error-free core loss can be recalculated similar to (6). For example, for the case in Fig. 6 at 50 kHz, the uncalibrated phase shift is found as 93.05 ns and the reference phase shift *PS_ref* is calculated as 69.90 ns. In this case, the *PS_Com* is 23.15 ns. After this manipulation, the compensated pair of inductor voltage and current can be considered to have a phase shift that is aligned to the physical phase shift.

Note between Figs. 9 and 4(b), the shapes of the measured and regenerated voltages show a slight difference, which is caused by the Fast Fourier Transform (FFT). Firstly, FFT ideally requires an integer number of cycles and no discontinuity at the endpoints of the data record [32], [33], which may not be perfectly satisfied in the studied segment. According to [34], there are also other possible sources of errors in FFT calculation such as (1) instability associated with factorization; (2) errors in the sine/cosine as twiddle factors; (3) roundoff errors. Secondly, the measured voltage waveform contains a wide range of harmonics, while the frequency range of FFT calculation is limited, which can be another source of error. Thirdly, the Gibbs phenomenon [35] in FFT is also a possible cause for this difference. The experimental voltage waveform contains asymmetric ringings and overshoots near the discontinuity. Depending on the harmonic order calculated, these ringings/overshoots are pushed to the discontinuity edge in the FFT process in a symmetric manner. Nevertheless, these FFT errors do not cause the relocation/shift of the zero-crossing point of regenerated voltage, since the before/after zero-crossings still overlap as we evaluated. In other words, although the shape of regenerated voltage shows a slight change, it does not affect the accuracy of the proposed approach in finding the reference phase angle.

In principle, the proposed approach is not sensitive to the dynamic inductance changes during the online testing (e.g., saturation at a high current level or dynamic permeability change), because the turning point of the current and zero-crossing point of the falling/rising edge of the inductor voltage are not changed for obtaining the *PD* of the proposed method in this case. Besides, this method is tied up to specific inductors (fixed core, winding, and inductance). For different inductor designs with different inductance, the impedance calibration needs to be redone. Additionally, the proposed method should be redone when the core properties are changed such as size and material, even if it leads to the same value of inductance. Since changing the core specification can affect the core and winding losses, these variations are reflected in the waveforms and the quality factor of the inductor, which leads to a different reference phase angle. There are many standardized inductors supplied these days, which means only one or a few representative samples need to be tested in this way to represent the property of a whole batch of inductors with the same core and winding arrangements [30].

Table 1 summarizes the phase variables involved in the proposed offline compensation method.

TABLE 1. Summary of Phase Variables

Physical Phase Shift *(PS)*	Real, physical phase shift in the measurement between I_{Pri} and V_{Sec}
Phase Discrepancy *(α)*	Phase discrepancy which comes from the instrument
Uncalibrated Phase Shift *(PD)*	$PD = PS + \alpha$ Extracted from experiment waveforms containing undesired phase discrepancy from the measurement instruments
Reference Phase Shift *(PS_Ref)*	Obtained from the proposed approach utilizing the impedance analyzer and FFT, which ideally suppresses α to zero
Phase Shift Compensation Offset *(PS_Com)*	$PS\_Com = PD - PS\_Ref$ To shift the raw waveform towards the reference phase shift

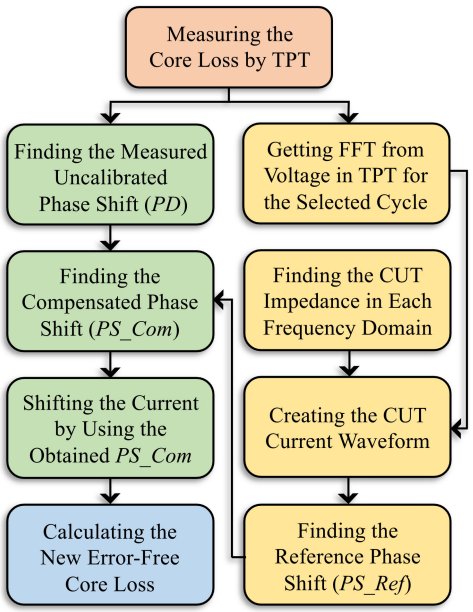

FIGURE 10. **The procedure of offline compensation of phase discrepancy.**

D. RECALCULATE CORE LOSS WITH THE PHASE DISCREPANCY COMPENSATED

With the phase shift of the current compensated, the core loss can be recalculated with the phase discrepancy error significantly reduced. Fig. 10 shows a flowchart, summarizing

TABLE 2. Experimental Results of Tested Core Loss, Offline Compensated Results Over Uncompensated Results

Frequency	Inductor 1 Iron Powder Difference (%)	Inductor 2 Ferrite N87 Difference (%)	Inductor 3 Ferrite N30 Difference (%)
10 kHz	-14.1859	----	----
20 kHz	-13.3163	-5.4460	----
30 kHz	-12.9258	-4.5624	-4.3261
40 kHz	-12.3934	-4.3283	-4.0189
50 kHz	-11.8915	-4.1888	-3.9865
60 kHz	-9.6557	-3.8544	-3.6311
70 kHz	-7.0615	-3.7350	-3.4880
80 kHz	-3.5188	-2.3022	-2.1367
90 kHz	3.5097	1.8822	1.5527
100 kHz	6.2613	3.6092	3.4152

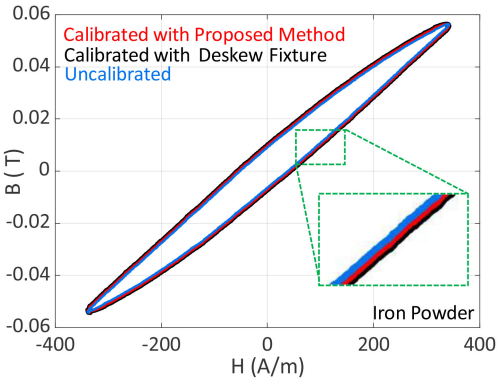

FIGURE 11. Experimentally measured *B–H* loops at 50 kHz for the Iron powder for three different cases, T = 25° C.

the whole process of the proposed approach. In short, the proposed method shifts the current waveform horizontally in the offline post-processing utilizing the reference phase shift *PS_Ref* found from the measured Z_L and *V* and the regenerated *i'*, in order to align to the physical phase shift *PS* and reduce the phase discrepancy error. The "offline" feature of the proposed approach is referring to where the phase discrepancy calibration is performed, for which the proposed method is performed in the post-processing stage after the measurement of the waveform has been completed with the main measuring/excitation equipment turned off. In comparison, the deskew method (e.g., using a calibration resistor/tool) is performed on the oscilloscope, which is perceived as an online deskew value (e.g., 5 ns). This feature of the proposed method means that the phase discrepancy problem does not need to be considered at the time of capturing the waveform, because it can be later compensated after the high-power measurement and excitation system is turned off.

Note the proposed method can also be applied for multilevel voltage waveforms, for which the calibration process would not be fundamentally different. Because the fundamental concept of the proposed approach is to align the voltage rising/ falling edge moments and the current turning point moments, for which the *PD* should be consistent for all the edges in multilevel voltage waveforms.

Table 2 illustrates the experimental comparison of offline compensated results against uncompensated results for three inductors tested with ±50V square wave and various frequencies, which are calculated by (11) in percentage, similar to (2).

$$\text{Difference} = \frac{\text{P}_{\text{Uncompensated}} - \text{P}_{\text{Compensated}}}{\text{P}_{\text{Compensated}}} \times 100\% \quad (11)$$

The results show that for inductor 1 with an iron powder core, the difference is more significant than the other two inductors with ferrite cores. The reason is that the microscopic air gaps distributed in the iron powder core material reduce its core permeability and increase the measurement sensitivity to the skew of probes according to equation (2) and (5). In contrast, the ferrite cores' permeability is higher than the iron powder core, which leads to less sensitivity to the probe skew in testing inductor 2 and 3. Similarly, the deviations in inductor 3 are better than inductor 2, because the permeability of N30 is higher than N87.

As the conventional approach, a deskew calibration can be performed on the oscilloscope before the testing, e.g., through a deskew fixture, Keysight U1880A. This conventional approach is compared with the proposed offline compensation method as shown in Fig. 11 depicting the *B–H* loops excited at 50 kHz frequency for inductor 1 with three cases: (1) uncalibrated (blue trace) (2) calibrated with deskew fixture (black trace) (3) calibrated with proposed method (red trace).

In this case, the obtained *PD* for the deskew case is about 0.035° (1.95 ns) leading from the *PS_Ref*, the value of the measured loss in the case calibrated with deskew fixture is larger than the case with offline compensation. By calculating the equation similarly to (6) for this case, the loss is corrected from 8.9 to 8.8 watt and the difference is at about 1.1%. However, if the iron powder core is not calibrated by the deskew tool, according to Table 2, the difference between uncompensated results and the offline compensated results at 50 kHz reaches 11.9%. This observation shows that the deskew tool can decrease the phase discrepancy to a degree that is very close to the proposed offline compensation method.

Fig. 12 depicts the compensated phase shift *PS_Com* (ns) in the tested cases with various excitation frequency for inductor 1. The results show the difference between the three compensation cases: (1) uncompensated (blue trace) (2) compensated with deskew fixture (black trace) (3) compensated with the proposed method (red trace, the reference). The results show that the proposed method and the deskew fixture method shows close compensation values, but they show different compensation manner at various frequencies. The proposed method should be considered more accurate in this case because it considers the frequency response across the spectrum. In contrast, the deskew fixture only performs the calibration with a fixed square wave featuring fixed rising/falling edge, amplitude and frequency.

[3] discussed that the phase response characteristics of different current probes (or current-sense resistors) vary at

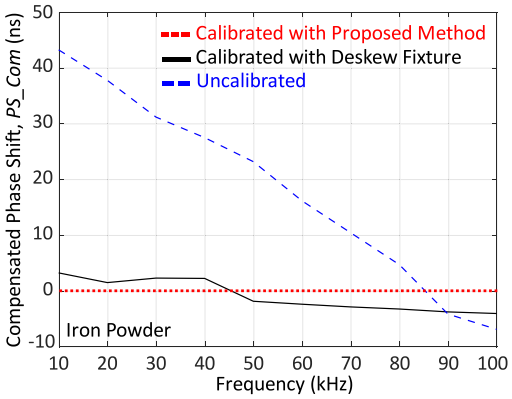

FIGURE 12. **Compensated phase shift *PS_Com* (ns) obtained from the proposed method for inductor 1 in the different cases, T = 25° C.**

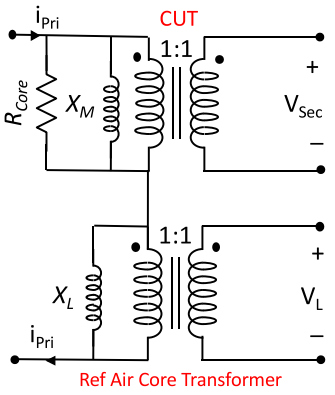

FIGURE 13. **Equivalent circuit of the partial inductive cancellation.**

various frequencies, which impacts the accuracy of the core loss measurement. According to equation (5) for one specific core, the core loss measurement is more sensitive to phase discrepancy error at low flux densities because of the presence of permeability in this equation [15]. Hence, for a particular frequency, the phase discrepancy error is different for various flux density values. Consequently, both the characteristics of the current probe and variation of the flux density affect the phase shift error in a nonlinear form across the frequency spectrum. Conventionally, phase compensations have been applied based on a linear error function with the frequency, similar to the deskew tool's case in Fig. 12. But, the phase error for each test has a nonlinear relationship with the frequency as also reported in [17], [18], and [3]. In contrast, the proposed method equivalently provides a non-linear compensation against various frequency as shown in Fig. 12, given the responses at various frequencies are captured in the impedance analyzer. The next section will validate the accuracy of the proposed method.

IV. EXPERIMENTAL VERIFICATION

In this section, with comparison to Hou's partial cancellation method presented in [10], the accuracy of the proposed method is verified. As one of the reactive voltage cancelling approaches introduced in section I, the fundamental concept of Hou's method is removing the reactive voltage of the CUT by using an air-core transformer, which reduces the phase difference between the CUT voltage and current from closely 90° to nearly 0°. Therefore, Hou's method is nearly immune to the phase discrepancy error, from which the results can be considered as the value that is closest to the physical loss. Hence, this work applies Hou's partial cancellation method to verify the proposed approach. Fig. 13 shows the equivalent circuit of the partial inductive cancellation method, which is utilized in this section.

For square voltage excitation in Hou's method, the core loss which is not sensitive to the phase discrepancy can be attained

TABLE 3. Parameters of the Inductor 4 and Air-Core Transformer

	Inductor 4	Air-Core
Toroidal Core		
Core Material	Iron Powder Material 26	Cardboard
Part Number	T184-26	-
Magnetizing Inductance	2 μH	0.9 μH
N=N1=N2	4	29
Volume *(mm³)*	21000	5300
Ae (mm²)	188	40
le (mm)	112	132

as follows (N_1=N_2)

$$P_{Core} = \frac{1}{T}\int_0^T i_{Pri}(t)\ .v_{Sec}(t)\ dt - \frac{1}{k}\frac{1}{T}\int_0^T i_{Pri}(t)\ .v_L(t)\ dt \tag{12}$$

$$k = \frac{V_{LP}}{V_{SecP}} \tag{13}$$

where k is the cancellation factor, which demonstrates the ratio of cancelled reactive voltage to the total reactive voltage. V_{LP} and V_{SecP} are the peak-to-peak values of v_L and v_{Sec} shown in Fig. 13, respectively.

To form the air-core transformer, the coils are wound on a plastic tube or cardboard, etc. An iron powder inductor (inductor 4) with relatively smaller inductance is measured by applying Hou's method with an air-core transformer, for which the parameters are listed in Table 3. The reason for using another inductor is due to the limitation of Hou's method that the CUT's magnetizing inductance must be small enough considering the matching air-core transformer's parasitic elements, which is discussed previously in section I.

By repeating the TPT, the core loss in various frequencies can be found at room temperature (T = 25° C) through the circuit in Fig. 13, (12), and components/instruments listed in Table 6. Fig. 14 depicts the experimental waveforms for the

TABLE 4. Experimental Results of the Iron Powder Core and the Air-Core Transformer in Proposed and Hou's Methods

Frequency	100 kHz	125 kHz	150 kHz
***PD* (ns)**	21.75	23.92	25.60
***PS_Ref* (ns)**	28.28	31.52	33.84
***PS_Com* (ns)**	-6.530	-7.600	-8.240
***PS_Com* (Degree)**	-0.235	-0.342	-0.445
Error Calculated from Proposed Method (%)	1.4	2.5	2.9
Dc-Bias Current	28 A	21.5 A	20.5A
Cancellation Factor (*k*)	0.39	0.40	0.42
Core Loss Before Proposed Phase Shift Method (W)	114	90.87	82.05
Core Loss After Proposed Phase Shift Method (W)	112.34	88.65	79.72
Core Loss in Hou's Method (W)	112.06	88.43	79.62
Differences Between Proposed Phase Shift Method and Hou's Method in (W) and (%)	0.273(W) 0.24 (%)	0.227(W) 0.26 (%)	0.102(W) 0.13 (%)

TABLE AI. Parameters of the Inductors

	Inductor 1	Inductor 2	Inductor 3
Toroidal Magnetic Core			
Core Material	Iron Powder Material 26	Soft Ferrite N87	Soft Ferrite N30
Part Number	T184-26	B64290L0084 X087	B64290A0084 X830
Rated Inductance	101µH	96 µH	94 µH
N=N1=N2	25	5	3
Volume *(mm³)*	21000	68220	68220
Ae (mm²)	188	267.2	267.2
le (mm)	112	255.3	255.3

TABLE AII. Components and Instruments in the Test Rig

Power Supplies	Elektro-Automatik TS 8000 T
Voltage Probe	Keysight N2862B (150 MHz)
Current Probe	Keysight N2783B (100 MHz)
Power Module	Semikron SKiM301TMLI12E4B
Gate Driver	Semikron SKYPER 42 J
Digital Oscilloscope	MSO-X 3054A (500 MHz, 4 GSa/s)
DC-Link Capacitance	$C1 = C2$ =2670 µF
DC-Link Voltage	100 V

test at 100 kHz frequency, which shows the voltages of the inductor 4 (v_{Sec}), air-core transformer (V_L), and the system current (i_{Pri}). Since the voltage probes are equivalent to each other, the phase delay between the two voltage channels can be ignored [2], [5].

Table 4 illustrates the results of the proposed method compared to Hou's method. Very low differences between the two methods are found below 0.3%, and the results at different frequencies show that the proposed method correctly follows

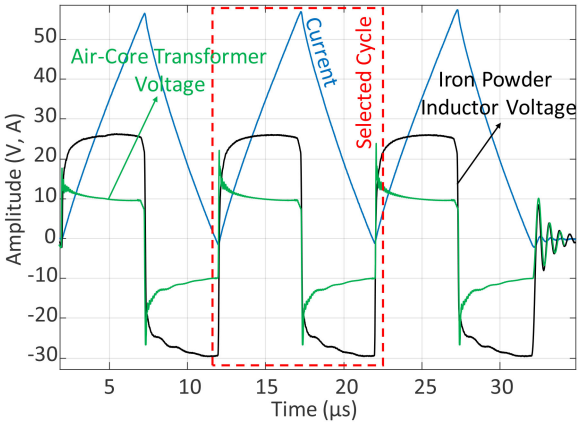

FIGURE 14. Experimental TPT waveforms for iron powder inductor and air-core transformer at 100 kHz frequency, T = 25° C.

Hou's method. The cancellation factor, in this case, is around 0.4 for each frequency, and as reported in [10], the maximum error that k can reach is about 0.4%, which is insignificant and neglectable. Note comparing to the inductor 1 case in Table 2, the uncompensated phase shift error is reduced in the inductor 4 case, because the actual phase (θ) of the inductor is decreased as it becomes lossier.

To prove that the dc-bias current amplitude does not affect the proposed method, the dc-bias current is changed to nearly zero in separate testings, in contrast to the three cases shown in Table 4. In these additional testings, the obtained *PS_Com* at nearly zero dc-bias current has a difference of less than 0.5 ns compared to the dc-biased case in Table 4 for the three tested frequencies. Also, the differences between the proposed method and Hou's method with and without the dc-bias current are all below 0.3%. At zero dc bias current, the relative differences compared to Hou's method are 0.25%, 0.24% and 0.15% in the tested 100, 125, and 150 kHz cases, respectively, which also asserted the accuracy of the presented method at a dc-biased case.

Overall, this comparison indicates that the proposed method can correctly compensate the phase discrepancy and yield an accurate core loss that is nearly identical to the results from Hou's method (<0.3% difference). As introduced, Hou's method is insensitive to the phase discrepancy and hence its results are considered as the most accurate baseline to verify the proposed approach. Although, Hou's method also has inherent errors such as the errors caused by the parasitic capacitance of the air-core transformer interwinding capacitance, and a voltage probe input capacitance, as discussed in [10]–[12]. It should be highlighted that the tested iron powder inductor has low permeability, while the proposed method still achieved small differences with respect to Hou's method.

One advantage of the proposed method is that it can be used when the magnetizing inductance of the CUT has higher values compared to Hou's method. Hou's method is limited to the cases with magnetizing inductances at a few hundreds of nano-henries, otherwise, the inductance would be too large for

the air-core transformer to match considering the parasitics. Therefore, the proposed method has superiority compared to the other reactive voltage cancellation methods for applications with typically up to a few hundred kilohertz, since power converter applications have comparably higher magnetizing inductances values in this case [36] (e.g., 50 $\sim$ 1000 μH). If the switching frequency of the converter is higher than a few MHz, it is typical to use air-cored inductors with no core loss to characterize. In applications with a high switching frequency (e.g., >10 MHz), the required inductance can be as small as 10 nH, such as the presented inductor in [37], which can be easily satisfied by coreless inductors. In this case, there is no core loss to measure, hence this context is not the targeted application background of the proposed method. The proposed approach only relies on the original component-under-test, which is typically a cored component with insignificant winding capacitance. An air-core transformer is avoided in the proposed approach in contrast to Hou's approach, while its parasitic elements can undermine the accuracy at the high-frequency range (e.g., >5 MHz).

Note the results in Table 4 covers harmonic components reaching the MHz range (similar to the case in Fig. 7), while the reactive cancellation method still highly agrees with the proposed approach. The main challenge in the MHz range for the proposed method is the effective frequency bandwidth of the measurement instruments to accurately capture the high-frequency characteristics in both the measured waveforms and the impedance sweep of the magnetic component. In theory, if the instruments are good enough, the proposed approach should offer high-precision compensation in any frequency range. Even if the fundamental frequency (i.e., the main switching frequency) of the square wave reaches 4 MHz, the significant harmonics (e.g., up to 30th) can still be captured by the 120 MHz impedance analyzer used in this work.

V. CONCLUSION

This paper has proposed a new approach to address the phase discrepancy issue in measuring the core loss with rectangular voltage. The proposed approach enables the engineers to accurately characterize the core loss with the two-winding method over a wide frequency range. A reference phase shift (*PS_Ref*) is found from an impedance frequency sweep on the magnetic-component-under-test to correct the horizontal position of the current waveform in the offline post-processing. Additionally, since the two-winding method can also be utilized to measure the copper loss and total loss of a magnetic component, this method is also valid in these contexts to decrease phase discrepancy error.

The proposed method is experimentally verified against the partial inductive cancellation method with and without the dc-bias condition, which shows consistent results. The main challenge for the proposed approach in the higher frequencies range (e.g., tens of MHz) is the effective frequency bandwidth of the measurement instruments, i.e., the voltage/current probes and the impedance analyzer. In summary, the proposed method features the following merits:

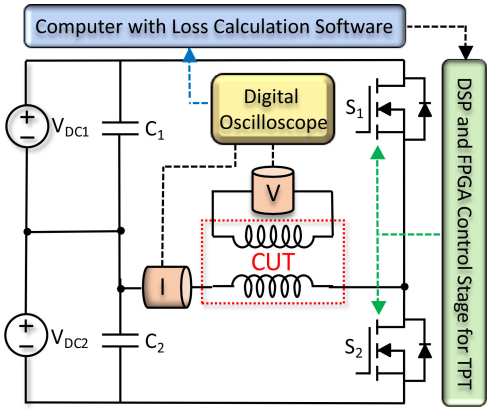

FIGURE AI. Simplified schematic of the power stage.

- Can be easily implemented to measure the error-free core losses exposed in rectangular excitation voltages.
- Waveform measurements can be done without considering the deskew at the time of measuring. The phase correction is conducted later in the offline post-processing as long as the magnetic component is preserved.
- Dynamic compensation against a wide frequency range.
- No need to build the cancelling component in the reactive voltage cancellation methods, such as the reference air-core transformer, low loss material transformer or compensation capacitors, which are associated with concerns on their parasitic elements.
- Fewer signals to measure, and has no limitation on excitation values and dc-biased current.

APPENDIX A. CORE LOSS MEASUREMENT AND SYSTEM SPECIFICATIONS

The measured data of secondary winding voltage and primary winding current are captured and post-processed by computer software, such as MATLAB, to found the core loss through expressions (A1)–(A3).

$$H(t) = \frac{N_1 \,.\, i_{Pri}(t)}{l_e} \tag{A1}$$

$$B(t) = \frac{1}{N_2 A_e} \int_0^T v_{Sec}(t)\, dt \tag{A2}$$

$$P_{Core} = \frac{N_1}{N_2} \frac{1}{T} \int_0^T i_{Pri}(t)\, .v_{Sec}(t)\, dt = A_e l_e \frac{1}{T} \int H\, dB \tag{A3}$$

To excite the CUT, a half-bridge structure is utilized and depicted in Fig. A1 [28]–[30]. This structure enables the compensation of the asymmetric square voltage caused by the device voltage drops, just by adjusting the output voltages of the two dc power supplies (V_{DC1} and V_{DC2}). The symmetric voltage excitation helps to form a closed *B-H* loop. The experiment setup is built and shown in Fig. A2, where the

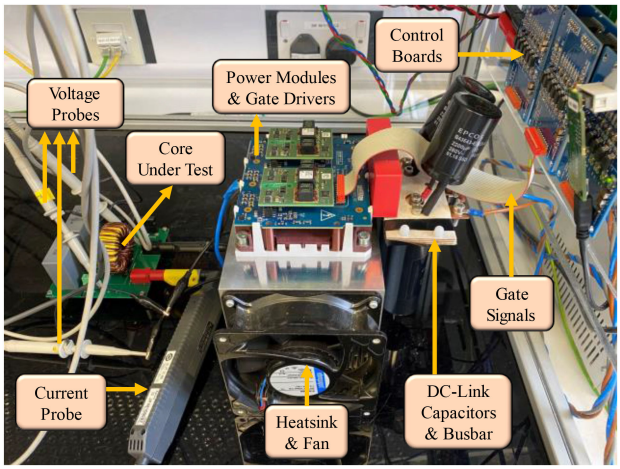

FIGURE AII. CUT in the test rig.

dc-link capacitors, busbars, power converter, control boards, and measurement probes are employed.

The utilized inductors with their specifications and the test rig components are listed in Table AI and Table AII, respectively.

APPENDIX B. REGENERATED MAGNETIC COMPONENT CURRENT

The virtually regenerated magnetic component current has been introduced in equation (10). It is realized by adding up all the current response of each frequency component given the inductor voltage and measured impedance. Hereunder is an explanation of this approach.

First of all, by performing fast Fourier transform (FFT), the amplitudes of each harmonic (n) of the inductor voltage ($V_{(n)}$) can be found for the selected cycle. The virtual square voltage waveform (v) displayed in Fig. 9 can be found by (A4) as

$$v = \sum_{n=1}^{n=\infty} \left[V_{(n)} \left[\sin\left(2\pi n f t\right) \right] + V_{(n)} \left[\cos\left(2\pi n f t\right) \right] \right] \quad \text{(A4)}$$

where f is the fundamental frequency and t is the time sample. If the square waveform is clean enough, the even harmonics are nearly zero and can be neglected.

The next step is to perform an impedance frequency sweep through an impedance analyzer. For instance, Fig. 8 shows the impedance of the iron powder Inductor 1 at each frequency ($Z_{L(n)}$), for which the impedance analyzer assumes the resistance (R) and inductance (L) are in parallel. Therefore, the magnitude of the impedance ($|Z|$) and its phase (φ) can be found for parallel form as

$$\frac{1}{Z_{L(n)}} = \frac{1}{R_{(n)}} + \frac{1}{j2\pi n f L_{(n)}} + j2\pi n f C_{(n)} \quad \text{(A5)}$$

$$|Z|_{(n)} = \frac{1}{\sqrt{\left(\frac{1}{R_{(n)}}\right)^2 + \left(\frac{1}{2\pi n f L_{(n)}} - 2\pi n f C_{(n)}\right)^2}} \quad \text{(A6)}$$

$$\emptyset_{(n)} = \tan^{-1}\left(R_{(n)}\left(\frac{1}{2\pi n f L_{(n)}} - 2\pi n f C_{(n)}\right)\right) \quad \text{(A7)}$$

Note the inductor has a winding capacitance (C) which according to [31], can be modelled in parallel form with the obtained magnetic component's resistance and inductance from the impedance analyzer. However, the winding parasitic capacitance in most cases is insignificant and can be ignored [4], [5] [8]–[10].

Regarding the winding resistance, it also contributes to the physical phase shift (PS) between the primary current and the magnetizing voltage in the online testing. Therefore, the winding resistance is included in the proposed offline impedance compensation to align the phase shift towards the physical value that occurred in the online testing.

Finally, after finding the impedance spectrum and the experimentally applied voltage on CUT, a triangular current i' on the inductor which is shown in Fig. 9 with its harmonics on each frequency $i'(n)$ can be virtually regenerated as

$$i' = \sum_{n=1}^{n=\infty} \frac{V_{(n)}}{Z_{L(n)}} = \sum_{n=1}^{n=\infty} \left[\left(\frac{V_{(n)}}{|Z|_{(n)}} \right) \left[\sin\left(2\pi n f t - \emptyset_{(n)}\right) \right] + \left(\frac{V_{(n)}}{|Z|_{(n)}} \right) \left[\cos\left(2\pi n f t - \emptyset_{(n)}\right) \right] \right] \quad \text{(A8)}$$

REFERENCES

[1] C. Xiao, G. Chen, and W. G. H. Odendaal, "Overview of power loss measurement techniques in power electronics systems," *IEEE Trans. Ind. Appl.*, vol. 43, no. 3, pp. 657–664, May–Jun. 2007.

[2] Y. Han, and Y. Liu, "A practical transformer core loss measurement scheme for high-frequency power converter," *IEEE Trans. Ind. Electron.*, vol. 55, no. 2, pp. 941–948, Feb. 2008.

[3] V. J. Thottuvelil, T. G. Wilson, and H. A. Owen, "High-frequency measurement techniques for magnetic cores," *IEEE Trans. Power Electron.*, vol. 5, no. 1, pp. 41–53, Jan. 1990.

[4] M. Mu, Q. Li, D. J. Gilham, F. C. Lee, and K. D. T. Ngo, "New core loss measurement method for high-frequency magnetic materials," *IEEE Trans. Power Electron.*, vol. 29, no. 8, pp. 4374–4381, Aug. 2014.

[5] Y. Han, W. Eberle, and Y. Liu, "A practical copper loss measurement method for the planar transformer in high-frequency switching converters," *IEEE Trans. Ind. Electron.*, vol. 54, no. 4, pp. 2276–2287, Aug. 2007.

[6] C. A. Baguley, B. Carsten, and U. K. Madawala, "The effect of dc bias conditions on ferrite core losses," *IEEE Trans. Magn.*, vol. 44, no. 2, pp. 246–252, Feb. 2008.

[7] Y. Han, G. Cheung, A. Li, C. R. Sullivan, and D. J. Perreault, "Evaluation of magnetic materials for very high frequency power applications," *IEEE Trans. Power Electron.*, vol. 27, no. 1, pp. 425–435, Jan. 2012.

[8] M. Mu, and F. C. Lee, "A new high frequency inductor loss measurement method," in *Proc. IEEE Energy Convers. Congr. Expo.*, Phoenix, AZ, 2011, pp. 1801–1806.

[9] M. Mu, F. C. Lee, Q. Li, D. Gilham, and K. D. T. Ngo, "A high frequency core loss measurement method for arbitrary excitations," in *Proc. 26th Annu. IEEE Appl. Power Electron. Conf. Expo.*, Fort Worth, TX, 2011, pp. 157–162.

[10] D. Hou, M. Mu, F. C. Lee, and Q. Li, "New high-frequency core loss measurement method with partial cancellation concept," *IEEE Trans. Power Electron.*, vol. 32, no. 4, pp. 2987–2994, Apr. 2017.

[11] F. Zhu, Q. Li, and F. C. Lee, "Improved partial cancellation method for high frequency core loss measurement," in *Proc. IEEE Appl. Power Electron. Conf. Expo.*, Anaheim, CA, USA, 2019, pp. 1430–1435.

[12] Z. Ma, J. Yao, Y. Li, and S. Wang, "Comparative analysis of magnetic core loss measurement methods with arbitrary excitations," in *Proc. IEEE Energy Convers. Congr. Expo.*, Baltimore, MD, USA, 2019, pp. 4125–4130.
[13] M. Mu, "High frequency magnetic core loss study," Ph.D. dissertation, Dept. Elect. Eng., Virginia Tech., Blacksburg, VA, USA, 2013.
[14] N. F. Javidi, and M. Nymand, "Error analysis of high frequency core loss measurement for low-permeability low-loss magnetic cores," in *Proc. IEEE 2nd Annu. Southern Power Electron. Conf.*, Auckland, 2016, pp. 1–6.
[15] N. F. Javidi, M. Nymand, and A. J. Forsyth, "New method for error compensation in high frequency loss measurement of powder cores," in *Proc. IEEE Appl. Power Electron. Conf. Expo.*, Tampa, FL, 2017, pp. 876–881.
[16] Keysight Technologies, "Keysight U1882B, Measurement Application for Infiniium Oscilloscopes", Dec. 2017, [Online]. Available: http://www.keysight.com/gb/en/assets/7018-01738/datasheets/5989-7835.pdf
[17] T. Shimizu, K. Kakazu, K. Takano, and H. Ishii, "Verification of iron loss calculation method using a high-precision iron loss analyzer," *IEEJ Trans. Ind. Appl.*, vol. 133, no. 1, pp. 84–93, 2013.
[18] H. Matsumori, T. Shimizu, K. Takano, and H. Ishii, "Evaluation of iron loss of ac filter inductor used in three-phase pwm inverters based on an iron loss analyzer," *IEEE Trans. Power Electron.*, vol. 31, no. 4, pp. 3080–3095, Apr. 2016.
[19] J. Muhlethaler, J. Biela, J. W. Kolar, and A. Ecklebe, "Core losses under the DC bias condition based on steinmetz parameters," *IEEE Trans. Power Electron.*, vol. 27, no. 2, pp. 953–963, Feb. 2012.
[20] T. Shimizu and S. Iyasu, "A practical iron loss calculation for AC filter inductors used in PWM inverters," *IEEE Trans. Ind. Electron.*, vol. 56, no. 7, pp. 2600–2609, Jul. 2009.
[21] L. Yi and J. Moon, "Direct in-situ measurement of magnetic loss in power electronic circuits," *IEEE Trans. Power Electron.*, vol. 36, no. 3, pp. 3247–3257, Mar. 2021.
[22] J. Moon, "In-situ direct magnetic loss measurement in a DC-DC converter," in *Proc. IEEE Energy Convers. Congr. Expo.*, Baltimore, MD, USA, 2019, pp. 1261–1268.
[23] C. R. Sullivan and J. H. Harris, "Testing core loss for rectangular waveforms, phase II final report," 2010. [Online]. Available: http://www.psma.com/coreloss/phase2.pdf
[24] K. Venkatachalam, C. R. Sullivan, T. Abdallah, and H. Tacca, "Accurate prediction of ferrite core loss with nonsinusoidal waveforms using only steinmetz parameters," in *Proc. IEEE Workshop Comput. Power Electron.*, 2002, pp. 36–41.
[25] C. R. Sullivan, J. H. Harris, and E. Herbert, "Core loss predictions for general PWM waveforms from a simplified set of measured data," in *Proc. IEEE Appl. Power Electron. Conf. Expo.*, 2010, pp. 1048–1055.
[26] C. R. Sullivan and J. H. Harris, "Testing core loss for rectangular waveforms," 2010. [Online]. Available: http://www.psma.com/coreloss/pilot.pdf
[27] E. Herbert, "Testing core loss for rectangular waveforms, phase II supplemental report," 2012. [Online]. Available: http://www.psma.com/coreloss/supplement.pdf
[28] J. Wang, K. J. Dagan, X. Yuan, W. Wang, and P. H. Mellor, "A practical approach for core loss estimation of a high-current gapped inductor in PWM converters with a user-friendly loss map," *IEEE Trans. Power Electron.*, vol. 34, no. 6, pp. 5697–5710, Jun. 2019.
[29] J. Wang, X. Yuan, and N. Rasekh, "Triple pulse test (TPT) for characterizing power loss in magnetic components in analogous to double pulse test (DPT) for power electronics devices," in *Proc. Annu. Conf. IEEE Ind. Electron. Soc.*, 2020, pp. 4717–4724.
[30] J. Wang, N. Rasekh, X. Yuan, and K. J. Dagan, "An analytical method for fast calculation of inductor operating space for high-frequency core loss estimation in two-level and three-level PWM converters," *IEEE Trans. Ind. Appl.*, vol. 57, no. 1, pp. 650–663, Jan./Feb. 2021.
[31] B. X. Foo, A. L. F. Stein, and C. R. Sullivan, "A step-by-step guide to extracting winding resistance from an impedance measurement," in *Proc. IEEE Appl. Power Electron. Conf. Expo.*, 2017, pp. 861–867.
[32] National Instruments Corporation, "Understanding FFTs and windowing," Mar 2019. [Online]. Available: http://www.ni.com./en-gb.html
[33] L. Chioye, "Choose the right FFT window function when evaluating precision ADCs," Nov 2013, [Online]. Available: http://www.electronicdesign.com
[34] J. C. Schatzman, "Accuracy of the discrete fourier transform and the fast fourier transform, "*SIAM J. Sci. Comput.*, vol. 17, no. 5, pp. 1150–1166, 1996.
[35] D. Morin, Fourier Analysis, Version 1, Nov. 2009, [Online]. Available: http://scholar.harvard.edu/files/david morin/files/waves_fourier.pdf
[36] B. Zhao, Q. Song, W. Liu, and Y. Sun, "Overview of dual-active-bridge isolated bidirectional DC-DC converter for high-frequency-link power-conversion system," *IEEE Trans. Power Electron.*, vol. 29, no. 8, pp. 4091–4106, Aug. 2014.
[37] W. Liang, L. Raymond, and J. Rivas, "3-D-printed air-core inductors for high-frequency power converters," *IEEE Trans. Power Electron.*, vol. 31, no. 1, pp. 52–64, 2016.

NAVID RASEKH (Student Member, IEEE) received the B.Sc. degree in electrical engineering from the Kermanshah University of Technology, Kermanshah, Iran, in 2015 and the M.Sc. degree in electrical engineering from the Amirkabir University of Technology, Tehran, Iran, in 2018. He is currently working toward the Ph.D. degree with the Electrical Energy Management Group, University of Bristol, Bristol, U.K. His main research interests include design and control of the power electronic converters, power loss modeling of magnetic components, wireless power transfer, and finite element analysis.

JUN WANG (Member, IEEE) received the B.S. degree in electrical engineering from Sichuan University, Chengdu, China, the M.Sc. degree in electrical engineering from the University of Nottingham, Nottingham, U.K., in 2014, and the Ph.D. degree in power electronics from the University of Bristol, Bristol, U.K., in 2019. He is currently a Senior Research Associate with the Electrical Energy Management Group, University of Bristol. His research interests include PWM power converters, multilevel DC or AC converter topologies, power loss modeling of power devices and magnetic components, and design optimization and application of wide-bandgap power devices.

XIBO YUAN (Senior Member, IEEE) received the B.S. degree in electrical engineering from the China University of Mining and Technology, Xuzhou, China, in 2005 and the Ph.D. degree in electrical engineering from Tsinghua University, Beijing, China, in 2010.

He has been a Professor since 2017 in the Electrical Energy Management Group, Department of Electrical and Electronic Engineering, University of Bristol, Bristol, U.K., where he became Lecturer, Senior Lecturer and Reader in 2011, 2015 and 2016, respectively. He also holds the Royal Academy of Engineering/Safran Chair in Advanced Aircraft Power Generation Systems. He is an executive committee member of the UK National Centre for Power Electronics and the IET Power Electronics, Machines and Drives (PEMD) network.

His research interests include power electronics and motor drives, wind power generation, multilevel converters, application of wide-bandgap devices, electric vehicles and more electric aircraft technologies. Professor Yuan is an Associate Editor of IEEE TRANSACTIONS ON INDUSTRY APPLICATIONS and IEEE JOURNAL OF EMERGING AND SELECTED TOPICS IN POWER ELECTRONICS. He is a Fellow of IET and received The Isao Takahashi Power Electronics Award in 2018.